Journal of Pharmaceutical and Biomedical Analysis 271 (2026) 117329

Contents lists available at ScienceDirect

Journal of Pharmaceutical and Biomedical Analysis

journal homepage: www.journals.elsevier.com/journal-of-pharmaceutical-and-biomedical-analysis

Rapid one-tube sputum processing for tuberculosis diagnosis via azide-functionalized magnetic nanoplatforms with selective bacterial capture

Bilsen Tural [a,b,*], Alican Bilden [c,f], Erdal Ertaş [b,d], Emre Tural [e], Hakan Temiz [f], Erdal Özbek [f], Servet Tural [a,b]

[a] Department of Nanotechnology, Institute of Science, Dicle University, Diyarbakir 21280, Turkey
[b] Department of Chemistry, Institute of Science, Dicle University, Diyarbakir 21280, Turkey
[c] Department of Medical Parasitology, Medical Faculty, Kırşehir Ahi Evran University, Kırşehir, Turkey
[d] Department of Food Processing, Technical Sciences Vocational School, Batman University, Batman, Turkey
[e] Faculty of Medicine, Department of Child Health and Diseases, Istanbul University-Cerrahpasa, Istanbul, Turkey
[f] Department of Medical Microbiology, Faculty of Medicine, Dicle University, Diyarbakir, Turkey

ARTICLE INFO

Keywords:
Tuberculosis diagnosis
Magnetic nanoparticles
Azide-functionalization
Sputum analysis
Magnetic separation
Ehrlich-Ziehl-Neelsen staining
Auramine-Rhodamine staining
Rapid TB detection

ABSTRACT

Tuberculosis (TB) remains a global health challenge requiring rapid and reliable diagnostic tools. Here, azide-functionalized magnetic nanoparticles (MNPs-N_3) were synthesized, characterized, and applied for one-tube detection of *Mycobacterium tuberculosis* (Mtb) in sputum. Structural analyses including Fourier-transform infrared (FT-IR), transmission electron microscopy (TEM), scanning electron microscopy (SEM), dynamic light scattering (DLS), and vibrating sample magnetometry (VSM) confirmed successful functionalization, uniform morphology, and preserved superparamagnetism. MNPs-N_3 were integrated into modified Ehrlich-Ziehl-Neelsen (MNPs-N_3-assisted EZN staining) and auramine-rhodamine (MNPs-N_3-assisted AR staining) staining protocols to enhance bacterial capture and visualization without decontamination or centrifugation. Control experiments using non-functionalized magnetic nanoparticles showed no bacterial co-localization, supporting the specificity of the azide-mediated interaction. The entire process was completed within one hour, offering a rapid alternative to conventional culture requiring $\geq$ 41 days. Using Mycobacterial Growth Indicator Tube (MGIT) culture as the reference, MNPs-N_3-assisted AR staining achieved 99 % sensitivity and 97 % specificity, outperforming MNPs-N_3-assisted EZN staining (95 % and 96 %, respectively). Diagnostic indices, including Youden index (0.96) and F1-score (0.98), demonstrated excellent agreement with culture results. These findings establish MNPs-N_3 as a fast, efficient, and cost-effective tool for Mtb diagnosis. The single-tube workflow minimizes contamination risk and simplifies laboratory handling, supporting potential application in resource-limited settings. Further optimization and large-scale clinical validation are still warranted.

1. Introduction

Tuberculosis (TB), caused by Mtb, remains a major global health concern, leading to significant morbidity and mortality, particularly in resource-limited settings [1]. Despite extensive efforts to control TB, the disease continues to pose a public health challenge, further exacerbated by the rise of drug-resistant strains [2]. Early and accurate diagnosis is critical for effective TB management; however, conventional diagnostic methods, including smear microscopy, culture, and nucleic acid amplification tests (NAATs), have notable limitations in sensitivity, specificity, and accessibility [3,4]. Smear microscopy, though widely used, suffers from low sensitivity, while culture-based methods, considered the gold standard, require prolonged incubation times, delaying timely treatment [5]. Although NAATs, such as GeneXpert Mtb/RIF, have improved diagnostic accuracy, their high cost and dependency on specialized equipment limit their use in low-resource settings [6,7]. These constraints highlight the need for alternative diagnostic strategies that are both rapid and reliable.

* Corresponding author at: Department of Nanotechnology, Institute of Science, Dicle University, Diyarbakir 21280, Turkey.
E-mail addresses: btural@dicle.edu.tr (B. Tural), alican.bilden@ahievran.edu.tr (A. Bilden), erdal.ertas@batman.edu.tr (E. Ertaş), emre.tural@iuc.edu.tr (E. Tural), hakan.temiz@dicle.edu.tr (H. Temiz), erdal.ozbek@dicle.edu.tr (E. Özbek), stural@dicle.edu.tr (S. Tural).

https://doi.org/10.1016/j.jpba.2025.117329
Received 25 September 2025; Received in revised form 24 December 2025; Accepted 28 December 2025
Available online 29 December 2025

One of the distinguishing features of Mtb is its unique cell wall composition, which differs from that of both Gram-positive and Gram-negative bacteria. The cell wall is rich in complex lipophilic glycolipids, including trehalose dimycolate (TDM) (also known as cord factor), trehalose monomycolate (TMM), and mycolic acids, which contribute to bacterial virulence and serve as specific biomarkers for TB detection [8–10]. Given their specificity to Mtb, targeting these cell wall components offers a promising approach for selective TB diagnosis [11].

Nanotechnology-based diagnostic approaches have emerged as powerful tools for enhancing sensitivity and specificity while reducing detection time [12,13]. Among these, magnetic nanoparticles (MNPs) have gained considerable attention due to their biocompatibility, ease of functionalization, and rapid magnetic separation capabilities [14]. Functionalized MNPs enable selective bacterial isolation from clinical samples, improving detection efficiency compared to conventional methods [15,16]. Specifically, surface-modified MNPs with functional chemical groups can selectively interact with bacterial components, providing a targeted and effective TB detection strategy [17].

In this study, we developed MNPs-N_3 designed to selectively bind Mtb. The azide (-N_3) functional group exhibits high nucleophilic reactivity, enabling strong interactions with mycobacterial cell wall components, particularly trehalose-containing glycolipids [18]. Previous studies have demonstrated that azide-modified trehalose analogs can be metabolically incorporated into the Mtb cell wall, further supporting the specificity of azide-functionalized systems for TB detection [19]. Additionally, azide groups have been widely utilized in bioorthogonal Click chemistry, facilitating covalent conjugation with alkyne-functionalized biomolecules for enhanced detection sensitivity [20,21].

By leveraging the unique properties of MNPs-N_3, we established a rapid, single-tube TB detection method that eliminates the need for conventional decontamination steps, significantly reducing diagnostic time while improving specificity and sensitivity. This study investigates the synthesis, characterization, and application of MNPs-N_3 for the selective capture of Mtb from sputum samples, providing a promising alternative to conventional TB diagnostic techniques [22–24].

2. Materials and method

2.1. Chemicals and materials

For tuberculosis diagnostic procedures, the TDC kit for decontamination and homogenization, Ehrlich-Ziehl-Neelsen (EZN) carbol fuchsin, Auramine-Rhodamine (AR) fluorochrome stain, methylene blue, and potassium permanganate were procured from RTA Laboratories Ltd. (Türkiye) and utilized in standard staining methods. The Mycobacterial Growth Indicator Tube (MGIT) system, including MGIT culture tubes, the Mycobacterium tuberculosis complex (MTBC) immunochromatographic cassette test, and the BACTEC MGIT 960 instrumentation, was supplied by BD Biosciences (USA).

Neodymium magnets (N52 grade) used for the selective isolation of MNPs-N_3-labeled bacteria were purchased from K&J Magnetics (USA). All aqueous solutions were prepared using ultrapure water (18.2 MΩ•cm) obtained from a Milli-Q water purification system (Merck Millipore, Germany). All chemicals and consumables were handled in accordance with standard laboratory safety procedures.

2.2. Synthesis and characterization of azide-modified magnetic nanoparticles (MNPs-N_3)

The synthesis of MNPs-N_3 was performed according to the method described in Tural et al. [25]. The synthesis mechanism of MNPs-N_3 is illustrated in Figure S1 (Supporting Information). The synthesized MNPs-N_3 nanoparticles were characterized using multiple analytical techniques to determine their structural, morphological, elemental, and surface properties. Morphology and surface structure were analyzed using scanning electron microscopy (SEM) with a QUANTA 400 F instrument, providing high-resolution imaging of the nanoparticles' external form and agglomeration behavior. Particle size and morphology were further examined using transmission electron microscopy (TEM) with a JEOL 2100F microscope, allowing high-magnification imaging to assess the nanoparticle core structure and aggregation state. The particle size distribution was measured using dynamic light scattering (DLS) with a Zetasizer Ultra Red Label instrument (Malvern Instruments Ltd, UK), which provided insights into size variation within nanoparticle agglomerates. Additionally, zeta potential measurements were performed using a Zetasizer Nano ZS instrument (Malvern Instruments Ltd, UK) at 25°C, determining the surface charge and stability of MNPs-N_3 in suspension. To identify functional groups present on the nanoparticle surface, Fourier transform infrared spectroscopy (FT-IR) analysis was conducted using a Perkin Elmer Mattson 1000 instrument equipped with an ATR (Attenuated Total Reflectance) accessory. The ATR-FT-IR spectra, recorded in the range of 4000–400 cm^{-1} , confirmed the successful functionalization of MNPs-N_3 by detecting characteristic absorption bands corresponding to azide groups and other surface modifications. These characterization techniques collectively validated the structural and functional properties of MNPs-N_3 for their application in tuberculosis detection.

2.3. Stability assessment of MNPs-N_3

The stability of MNPs-N_3 was evaluated under refrigerated storage conditions (4 °C) for up to two weeks. After synthesis, the nanoparticles were thoroughly washed with deionized water to remove unreacted precursors and by-products. The washed samples were subsequently freeze-dried (FreeZone 2.5 L, Labconco, USA) to obtain dry powders for FT-IR and VSM analyses. Prior to storage, the dried samples were transferred into light-proof glass containers, purged with high-purity nitrogen gas to create an inert atmosphere, and hermetically sealed. The sealed containers were then stored at 4 °C until further use.

For DLS analysis, freshly washed (wet) MNPs-N_3 suspensions were used. Following the washing step, the samples were similarly purged with nitrogen gas, sealed in light-protected tubes, and stored at 4 °C to prevent oxidation or photochemical degradation. All measurements were performed using samples withdrawn directly from the refrigerated stock without additional purification steps.

2.4. Sample collection and processing

Sputum samples were collected from patients with suspected TB at the Dicle University Faculty of Medicine, Department of Medical Microbiology, Mycobacteriology Laboratory. A total of 565 sputum samples were included in the study. Ethical approval was obtained, and all patients provided informed consent prior to sample collection. Samples were collected in sterile, leak-proof polypropylene containers and stored at 2–8 °C until analysis.

To ensure a uniform processing workflow for the comparative evaluation of all diagnostic methods, sputum samples were decontaminated, homogenized, and concentrated using the TDC kit (RTA Laboratories Ltd., Türkiye). The procedure involved adding an equal volume of 4 % sodium hydroxide (NaOH), followed by N-acetyl-L-cysteine (NALC) treatment for 15 min. The pH was then neutralized using phosphate buffer, and mycobacteria were concentrated via centrifugation. The resulting pellet was used for conventional staining and MGIT culture.

Although the MNPs-N_3 method does not inherently require decontamination, TDC processing was applied to all samples in this study to maintain methodological consistency across all diagnostic techniques and allow direct performance comparison.

2.5. Tuberculosis diagnostic methods

Sputum samples were analyzed using conventional and MNPs-N_3-modified staining techniques. EZN staining was performed using

standard procedures, including heat fixation, carbol fuchsin staining, acid-alcohol decolorization, and counterstaining with methylene blue. Auramine-Rhodamine fluorescent staining was performed using AR fluorochrome staining, acid-alcohol decolorization, and counterstaining with potassium permanganate. MNPs-N_3-based staining techniques (MNPs-N_3-assisted EZN staining and MNPs-N_3-assisted AR staining) involved selective isolation of Mtb using neodymium magnets, removal of the supernatant, and direct staining of the isolated pellet.

2.6. Culture-based methods

MGIT (Mycobacterial Growth Indicator Tube) culture was conducted by inoculating processed samples into MGIT tubes and incubating them in the BACTEC MGIT 960 system for up to 45 days. Positive cultures were confirmed using EZN staining and immunochromatographic assays (Mtb identification strip test).

2.7. Application of MNPs-N_3 for TB detection

MNPs-N_3 (10 mg) was added to 0.5 mL of processed sputum samples in a single tube, followed by gentle mixing and incubation for 10 min to allow interaction with Mtb. After incubation, neodymium magnets were used to isolate MNPs-N_3-Mtb aggregates. The supernatant was discarded, and the pellet remained in the same tube for subsequent staining procedures.

To evaluate the specificity of azide-mediated bacterial capture, unmodified Fe_3O_4 nanoparticles (lacking azide groups) were included as a negative control. The Fe_3O_4 nanoparticles were subjected to the same workflow as MNPs-N_3, including incubation with processed sputum samples, magnetic separation, and subsequent EZN or AR staining. No additional protocol modifications were applied for the negative control.

For MNPs-N_3-assisted EZN staining, carbol fuchsin was directly added to the pellet inside the tube and heated for 4–5 min. The pellet was then washed, and decolorization was performed by adding 3 % acid-alcohol for 30 s. The supernatant was removed using a pipette, and no further counterstaining with methylene blue was applied, differing from the conventional EZN technique. After completing the staining process, 0.5 μL of the stained sample was transferred onto a slide, air-dried, and examined under a light microscope at 100x magnification using immersion oil, covering approximately 300 fields.

For MNPs-N_3-assisted AR staining, the same procedural steps were followed, except no heating was applied during the staining process. Unlike the conventional method, the MNPs-N_3-based approach did not require an initial decontamination step before staining.

2.8. Statistical analysis

The diagnostic performance of MNPs-N_3-based TB detection methods was evaluated using sensitivity, specificity, positive predictive value (PPV), negative predictive value (NPV), and overall accuracy. McNemar's test, Cohen's kappa, Youden index, and F1-score were used to assess agreement with the MGIT gold standard and other diagnostic techniques (Table 2). Likelihood ratios (LR+ and LR−), diagnostic odds ratio (DOR), Matthews correlation coefficient (MCC), and balanced accuracy were determined for further evaluation (Table 3, Table 4). Net reclassification improvement (NRI) and decision curve analysis (DCA) were performed to assess the clinical utility of MNPs-N_3-based methods. The overall workflow of the single-tube MNPs-N_3 tuberculosis detection process is illustrated in Fig. 1A. The staining-based microscopic confirmation of selective Mtb capture obtained after magnetic isolation is presented in Fig. 1B. Statistical significance was set at $p < 0.05$, and analyses were conducted using SPSS software (version 23, IBM Corp., USA) and GraphPad Prism (version 10, GraphPad Software, USA).

3. Results

3.1. Characterization of MNPs-N_3

The morphological properties of MNPs-N_3 were characterized by transmission and scanning electron microscopy. TEM images (Fig. 2A) revealed uniformly distributed, spherical nanoparticles with diameters ranging from 5 to 10 nm. SEM micrographs (Fig. 2B) demonstrated moderate aggregation attributed to magnetic dipole-dipole interactions, consistent with the superparamagnetic behavior of the particles. These results confirm the successful synthesis and structural uniformity of MNPs-N_3 [26]. Additional physicochemical characterization data provided in the Supplementary Materials (Fig. S2–S3) further validate the successful azide functionalization of the magnetic nanoparticles and confirm that the resulting MNPs-N_3 possess the structural and physicochemical properties required for the subsequent biological capture experiments.

3.2. Stability and physicochemical evaluation

The structural and physicochemical stability of azide-functionalized magnetic nanoparticles (MNPs-N_3) was investigated by FT-IR, DLS, and VSM (Fig. 3 (A, B, C)) analyses immediately after synthesis and following two weeks of refrigerated storage (4 °C).

Table 2
Statistical comparison of MNPs-N_3 methods and other diagnostic techniques.

Method Comparison	McNemar Test (p-value)	Cohen's Kappa	Youden Index	F1-Score
MGIT vs. MNPs-N_3 (EZN)	0.0	0.91	1.0	0.96
MGIT vs. MNPs-N_3 (AR)	0.25	0.96	1.0	0.98
EZN Staining vs. MNPs-N_3 (EZN)	0.0	0.3	0.25	0.51
AR Staining vs. MNPs-N_3 (AR)	0.0	0.65	0.64	0.81

Table 1
Diagnostic performance of different mtb detection methods compared to the MGIT gold standard.

Test Method	True Positive (TP)	True Negative (TN)	False Positive (FP)	False Negative (FN)	Sensitivity	Specificity	Positive Predictive Value (PPV)	Negative Predictive Value (NPV)	Accuracy
MGIT	315	250	0	0	1	1	1	1	1
Mtb ICA	289	225	25	26	0.92	0.90	0.920	0.90	0.91
EZN Staining	99	233	17	216	0.31	0.93	0.85	0.52	0.59
MNPs-N_3 (EZN)	299	241	9	16	0.95	0.96	0.97	0.94	0.96
AR Staining	214	239	11	101	0.68	0.96	0.95	0.70	0.80
MNPs-N_3 (AR)	312	243	7	3	0.99	0.97	0.98	0.99	0.98

Table 3
Advanced statistical evaluation of MNPs-N_3 methods for Mtb diagnosis.

Method Comparison	LR+	LR-	DOR	NRI	Net Benefit (DCA)
MGIT vs. MNPs-N_3 (EZN)	26.37	0.05	500.41	-0.09	0.91
MGIT vs. MNPs-N_3 (AR)	35.37	0.01	3610.29	-0.04	0.96
EZN vs. MNPs-N_3 (EZN)	26.37	0.05	500.41	0.67	0.91
AR Staining vs. MNPs-N_3 (AR)	35.37	0.01	3610.29	0.33	0.96

FT-IR spectra (Fig. 3A) revealed the characteristic Fe-O stretching vibration of the magnetite core at 542 cm^{-1}, Si-O-Si asymmetric stretching bands at 798 and 1071 cm^{-1} corresponding to the silica shell, and a distinct azide (-N_3) stretching band at 2101 cm^{-1}, confirming successful surface modification. The positions and intensities of these peaks remained unchanged after two weeks of storage, indicating excellent chemical stability and preservation of surface functional groups [27–29].

Dynamic light scattering (DLS) analysis (Fig. 3B) demonstrated a narrow particle size distribution, with an average hydrodynamic diameter of approximately 500 nm immediately after synthesis and less than 5 % variation following two weeks of storage. The zeta potential remained around −32 mV, suggesting stable electrostatic repulsion and minimal aggregation over time [28].

Vibrating sample magnetometry (VSM) analysis (Fig. 3C) confirmed that the nanoparticles retained their superparamagnetic behavior, exhibiting no coercivity or remanence. The saturation magnetization (Ms) slightly decreased from 38.3 emu/g (freshly prepared) to 37.1 emu/g after storage, which can be attributed to minor surface reorientation of the silica and azide layers. This marginal change does not affect the magnetic responsiveness required for efficient magnetic separation [26].

Collectively, these results demonstrate that MNPs-N_3 nanoparticles maintain their structural, colloidal, and magnetic integrity for at least two weeks under standard refrigerated conditions. The preservation of azide functional groups and stable physicochemical behavior support their reproducibility and practical suitability for diagnostic applications.

Importantly, the long-term stability of the azide surface functionality ensures that the nanoparticles retain their ability to interact with Mtb cell-wall glycolipids, a key requirement for consistent bacterial capture. The minimal variation in particle size and surface charge further supports reliable performance across different batches and storage periods, strengthening the translational potential of MNPs-N_3 for routine TB diagnostics.

3.3. Microscopic evaluation of MNPs-N_3 interactions with sputum

Fig. 4A presents the EZN-stained microscopic images of MNPs-N_3, comparing their behavior without sputum interaction and after interaction with sputum. In the absence of biological material, MNPs-N_3 formed dense aggregates with a relatively uniform distribution, and no acid-fast structures were visible, indicating that the nanoparticles alone do not exhibit staining features typical of Mtb. In contrast, when MNPs-N_3 was applied to sputum samples before EZN staining, acid-fast bacilli stained in characteristic reddish-pink were clearly observed within the nanoparticle clusters. This co-localization demonstrates that MNPs-N_3 effectively interacts with Mtb in sputum, enabling selective bacterial isolation and enhanced microscopic visualization.

Similarly, Fig. 4B shows AR-stained microscopic images of MNPs-N_3. Without sputum interaction, MNPs N_3 aggregates appeared as non-specific dense clusters that lacked any fluorescent structures. However, when incubated with sputum prior to AR staining, bright yellow green fluorescent bacilli, which are characteristic of Mtb under fluorescence microscopy, became clearly distinguishable within the MNPs N_3 aggregates. This finding confirms that MNPs N_3 promotes selective bacterial retention and enhances fluorescence based visualization efficiency.

Importantly, Fig. 4C shows the corresponding microscopic image obtained using non-functionalized Fe_3O_4 nanoparticles under identical staining conditions. In this negative control, no co-localization with acid-fast bacilli was observed in either EZN or AR staining. The absence of bacterial binding by Fe_3O_4 alone confirms that the selective interaction observed in Fig. 4A-B is attributable to the azide functional groups on MNPs-N_3 rather than nonspecific magnetic aggregation. Additional microscopic images supporting these observations, including cord formation and fluorescence-based validation of the MNPs-N_3-Mtb complex, are provided in Supplementary Fig. S4.

3.4. Diagnostic performance comparison

A total of 565 sputum samples were analyzed using conventional and MNPs-N_3-based TB diagnostic techniques. The performance of each method was evaluated in terms of sensitivity, specificity, positive predictive value (PPV), negative predictive value (NPV), and overall diagnostic accuracy (Table 1, Fig. 1).

Among the conventional methods, EZN staining showed a sensitivity of 31 % and specificity of 93 %, which is consistent with previous reports indicating a wide sensitivity range (3.3–70 %) [30]. AR fluorescence staining provided a higher sensitivity of 68 %, with a specificity of 96 % [31]. The statistical evaluation of these methods is presented in Fig. 5A, which illustrates their diagnostic performance in terms of the Youden index.

Molecular and culture-based diagnostic techniques demonstrated improved performance. The MGIT culture method, used as the gold standard, identified TB-positive cases with 100 % sensitivity and specificity but required a minimum of 41 days for final results [32]. The Mtb Immunochromatographic assay (ICA) test, an immunochromatographic assay, exhibited a sensitivity of 92 % and specificity of 90 % [33].

In contrast, MNPs-N_3-based diagnostic methods significantly improved both sensitivity and specificity. The MNPs-N_3-assisted EZN staining method demonstrated a sensitivity of 95 % and specificity of 96 %, while MNPs-N_3 (AR) achieved a sensitivity of 99 % and specificity of 97 % (Table 1). The ROC curve analysis (Fig. 5B) illustrates that the MNPs-N_3-based methods showed diagnostic performance comparable to molecular methods, with high area under the curve (AUC) values. The Youden index values presented in Table 2 further emphasize the superior discriminatory power of MNPs-N_3 compared to conventional staining techniques.

Unlike conventional staining techniques, the MNPs-N_3-based approach allowed selective bacterial isolation within a single tube, eliminating the need for decontamination steps such as NaOH/NALC treatment [34]. The direct bacterial capture by MNPs-N_3 significantly reduced sample loss and improved detection efficiency. Furthermore,

Table 4
Statistical evaluation of Mtb diagnostic performance: MCC, FDR, and likelihood Ratios.

Method Comparison	MCC	Balanced Accuracy	Prevalence	Disease Detection Rate	FDR	LR+ CI (Lower, Upper)	LR- CI (Lower, Upper)
MGIT vs. MNPs-N_3 (EZN)	0.91	0.96	0.56	0.95	0.03	25.74 27.01	25.70 27.05
MGIT vs. MNPs-N_3 (AR)	0.96	0.98	0.56	0.99	0.02	34.64 36.13	34.99 35.76
EZN Staining vs. MNPs-N_3 (EZN)	0.91	0.96	0.56	0.95	0.03	25.74 27.01	25.70 27.05
AR Staining vs. MNPs-N_3 (AR)	09.6	0.98	0.56	0.99	0.02	34.64 36.13	34.99 35.76

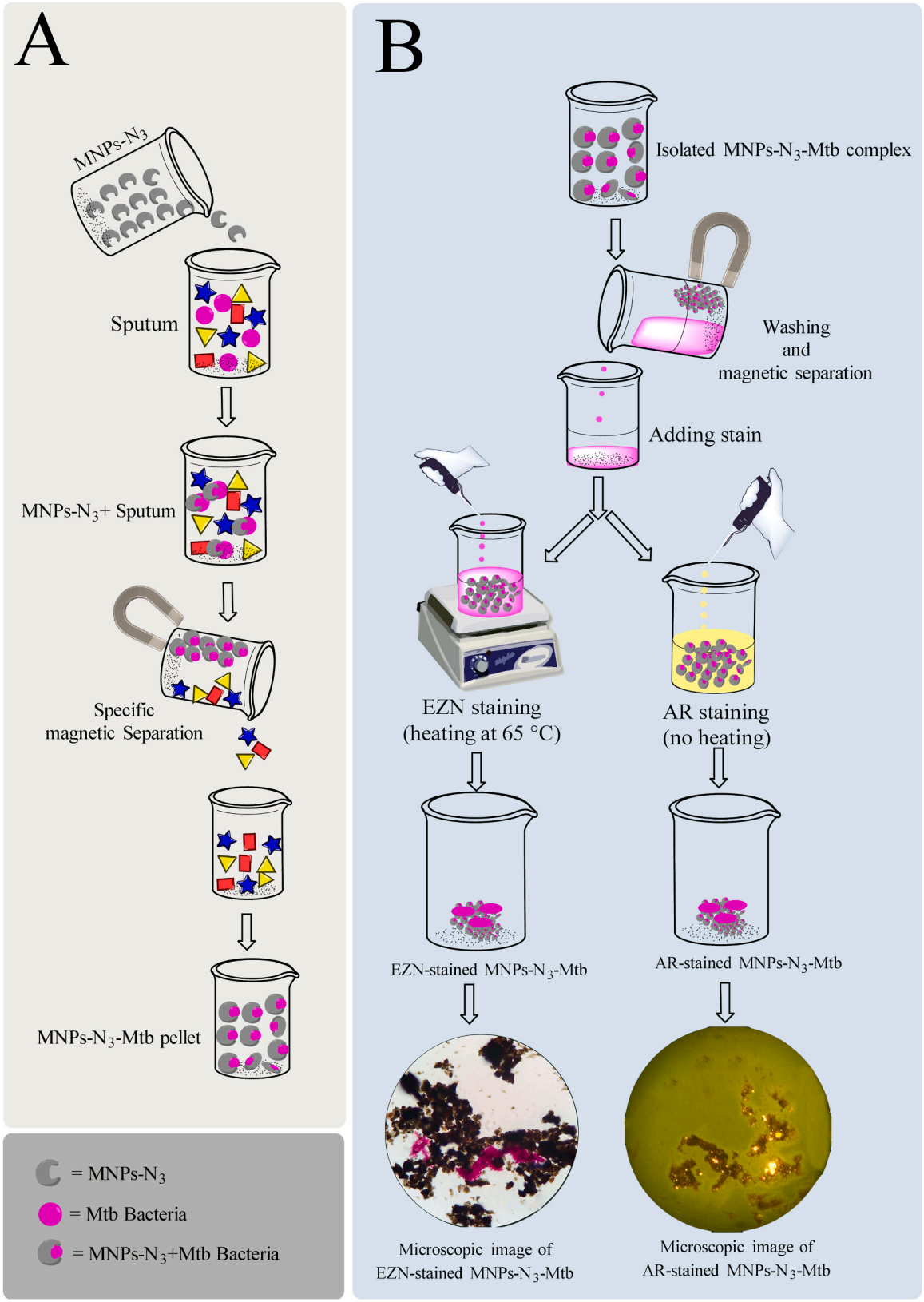

Fig. 1. One-tube azide-functionalized magnetic nanoparticle (MNPs-N₃) workflow and staining-based confirmation of selective Mtb capture. (A) Schematic overview of the single-tube MNPs-N₃ workflow, illustrating the addition of azide-functionalized magnetic nanoparticles to sputum, incubation, magnetic isolation of MNPs-N₃-Mtb complexes, and retention of the pellet within the same tube. (B) Direct EZN or AR staining of the isolated pellet inside the tube, enabling co-localized visualization of acid-fast bacilli and confirming the selective binding capability of the MNPs-N₃ platform.

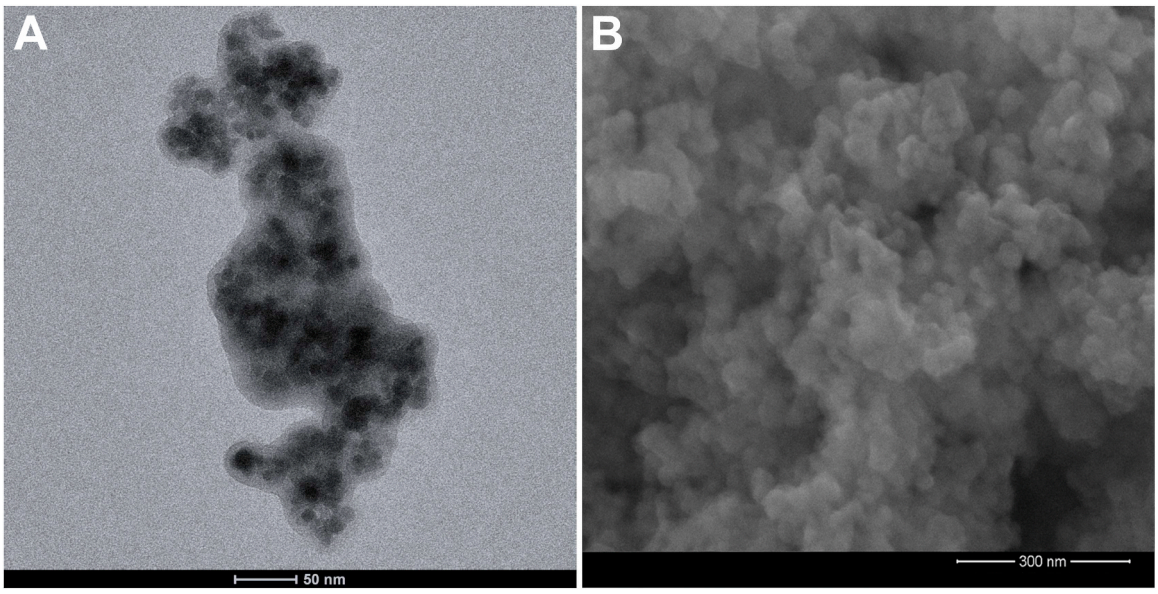

Fig. 2. TEM (A) and SEM (B) images of azide-functionalized magnetic nanoparticles (MNPs-N_3).

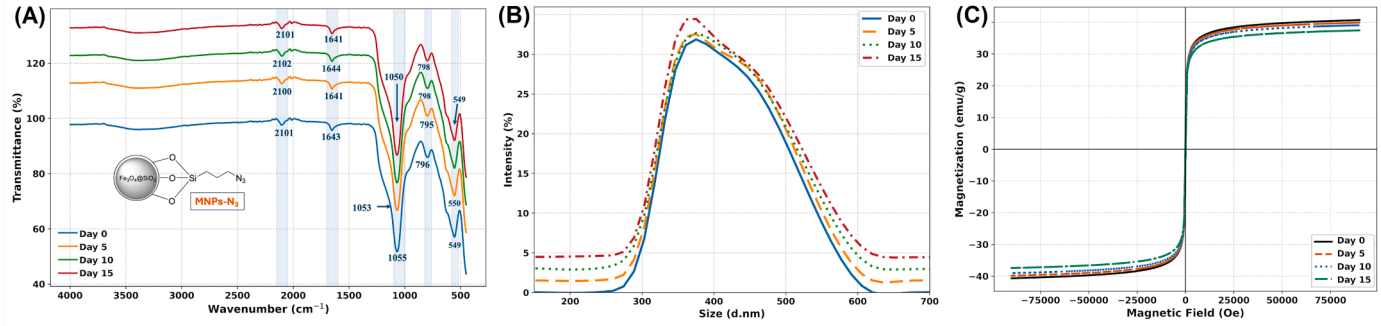

Fig. 3. Stability assessment of azide-functionalized magnetic nanoparticles (MNPs–N_3) by FTIR, DLS, and VSM analyses. **(A)** FTIR spectra of MNPs–N_3 recorded on Day 0, Day 5, Day 10, and Day 15 during storage at 4 °C. The preserved azide stretching band at approximately 2100 cm^{-1} and the absence of significant spectral shifts indicate stable surface functionalization and negligible structural degradation over the 15-day period. **(B)** Dynamic light scattering (DLS) size distribution profiles of MNPs–N_3 measured over the same storage period, showing minimal variation in hydrodynamic diameter and confirming colloidal stability. **(C)** Vibrating sample magnetometry (VSM) curves of MNPs–N_3 recorded from Day 0 to Day 15, demonstrating preserved superparamagnetic behavior and only minor changes in magnetic saturation, indicating stable magnetic properties throughout storage.

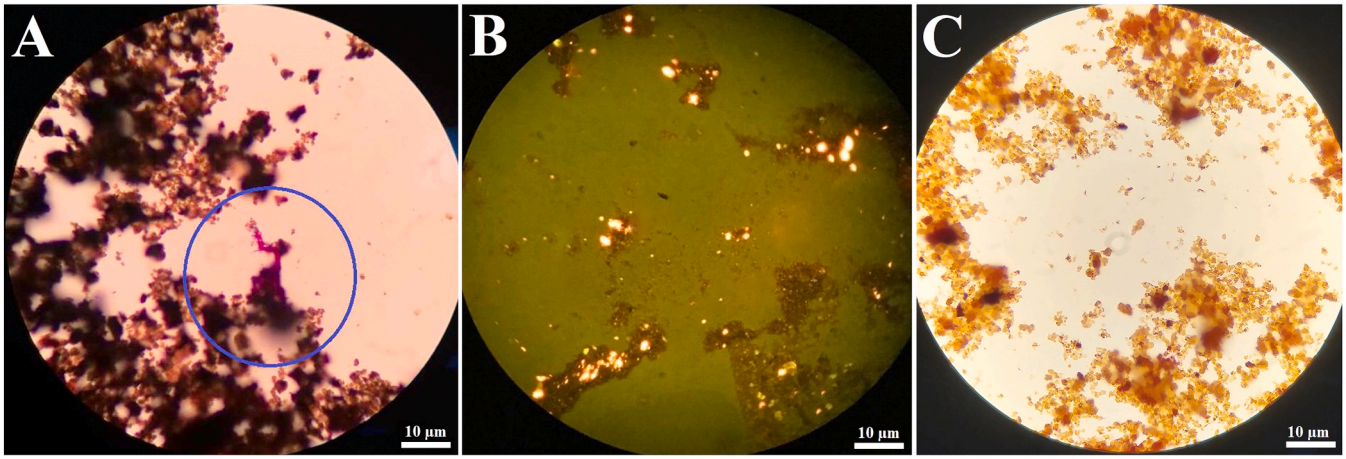

Fig. 4. Microscopic evaluation of MNPs-N_3-Mtb complexes under EZN and AR staining. (A) EZN-stained MNPs-N_3-Mtb complex showing acid-fast bacilli (highlighted by a circle) bound to nanoparticle aggregates. (B) Fluorescence image of AR-stained MNPs-N_3-Mtb complex, demonstrating bright yellow-green fluorescence typical of *Mycobacterium tuberculosis*. (C) Non-functionalized Fe_3O_4 nanoparticles processed with EZN staining, showing absence of acid-fast bacilli (negative control).

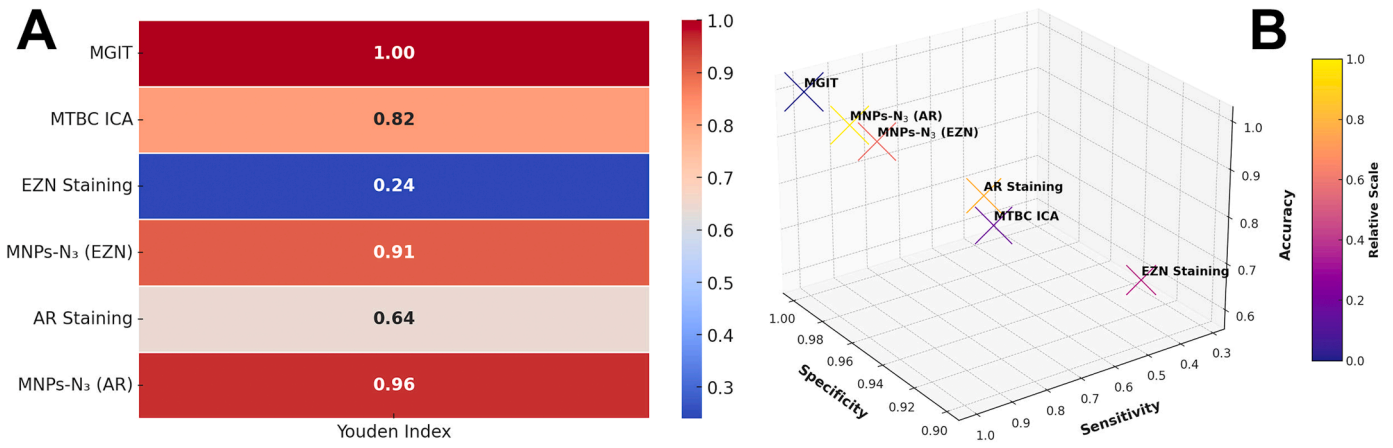

Fig. 5. Performance Analysis of TB Diagnostic Tests: (A) Youden Index and (B) 3D Diagnostic Performance Mapping.

conventional EZN staining required counterstaining with methylene blue, while MNPs-N₃-assisted EZN staining did not, making the process more streamlined and efficient. Similarly, MNPs-N₃-assisted AR fluorescence staining eliminated the need for heating, further simplifying the procedure. The diagnostic improvement provided byMNPs-N₃ is visually represented in the 3D Bubble Chart (Fig. 5B), demonstrating the correlation between specificity, sensitivity, and diagnostic accuracy.

Together, these findings confirm that MNPs-N₃ significantly enhances both analytical sensitivity and operational efficiency, addressing several limitations of routine smear microscopy and offering a practical alternative for high-burden, resource-limited settings.

3.5. Statistical validation and advanced analysis

Advanced statistical analyses further confirmed the high diagnostic reliability of the MNPs-N₃ approach. The diagnostic odds ratio (DOR) for MNPs-N₃ (AR) was 3610.29, indicating a significantly higher discriminatory power compared to conventional staining methods (Table 3). Additionally, the Matthews Correlation Coefficient (MCC) for MNPs-N₃ (AR) was 0.96, reflecting strong agreement with the MGIT gold standard (Table 4).

Furthermore, the positive likelihood ratio (LR+) for MNPs-N₃ (AR) was 35.37, while the negative likelihood ratio (LR-) was only 0.01, highlighting the method's ability to confidently predict both TB-positive and TB-negative cases.

These findings are further illustrated in Fig. 5, where the ROC curves and 3D bubble chart collectively demonstrate the superior balance of sensitivity, specificity, and diagnostic accuracy achieved by the MNPs-N₃ platform.

Taken together, the statistical analyses reinforce that MNPs-N₃ substantially outperforms conventional staining techniques and provides diagnostic metrics that approach those of molecular assays, while maintaining operational simplicity and rapid turnaround.

3.6. Mechanistic insights, literature context, and clinical implications

The selective capture of Mtb by MNPs-N₃ can be explained by the distinctive biochemical architecture of the mycobacterial cell envelope. Mtb possesses a lipid-rich and highly hydrophobic outer layer dominated by long-chain mycolic acids, trehalose-based glycolipids, and complex polysaccharides that are absent in most other bacterial species [31–34]. Among these, TDM and TMM function as major virulence-associated glycolipids and contribute to the unique permeability and immunomodulatory properties of the pathogen [35–40]. These biomolecular constituents form a structurally dense and chemically reactive interface, providing a favorable environment for physicochemical interactions with surface-modified nanomaterials.

In this context, azide functionality plays a critical role in facilitating bacterial capture. Previous studies have shown that azide groups can associate with trehalose-mycolate structures and other glycolipid-rich surfaces through non-covalent interactions and click-compatible affinity processes [41]. This mechanistic framework is consistent with our experimental findings: while azide-functionalized MNPs-N₃ demonstrated robust co-localization with acid-fast bacilli, unmodified Fe_3O_4 nanoparticles showed no detectable interaction, confirming the essential role of azide surface chemistry in selective binding. These mechanistic observations complement established diagnostic practices, including MGIT-based culture systems for mycobacterial detection [42], and align with the growing need for rapid, point-of-care TB diagnostic platforms [43]. Collectively, these results support the mechanistic validity and translational potential of the MNPs-N₃-based workflow as an alternative rapid diagnostic approach.

4. Conclusion

In summary, this study presents a rapid, reliable, and cost-effective diagnostic approach for tuberculosis using MNPs-N₃. The developed one-tube method enables selective bacterial capture and microscopic visualization within one hour, demonstrating superior diagnostic accuracy compared with conventional staining and culture techniques. The integration of azide chemistry with magnetic separation provides a practical, low-cost, and contamination-free workflow that is particularly suitable for routine clinical microbiology laboratories.

However, this study has certain limitations. The interaction mechanism between the azide groups and the Mtb cell-wall glycolipids was inferred based on physicochemical characterization and literature evidence but not yet validated at the molecular level. In the current revision, we addressed this limitation by introducing a negative control group (non-functionalized Fe_3O_4), which demonstrated the absence of bacterial co-localization. This newly added control supports the azide-mediated interaction mechanism within a clinically relevant sputum environment. Additionally, although 565 clinical sputum samples were analyzed, further validation on a larger and more diverse population would enhance clinical applicability. Future studies will also focus on complementary biophysical or biochemical assays that are compatible with complex clinical matrices to further support the mechanistic interpretation.

Future work will focus on molecular confirmation of the interaction mechanism and the integration of this platform with automated optical readout systems for large scale screening. Overall, the proposed MNPs N₃ platform represents a promising advancement toward a rapid and fully single tube tuberculosis diagnostic tool that can be adapted to low resource settings.

CRediT authorship contribution statement

Alican Bilden: Writing – review & editing, Writing – original draft, Methodology, Investigation. **Bilsen Tural:** Writing – review & editing, Writing – original draft, Visualization, Validation, Supervision, Methodology, Investigation, Funding acquisition, Formal analysis, Conceptualization. **Emre Tural:** Writing – review & editing, Writing – original draft, Methodology, Investigation. **Erdal Ertaş:** Writing – review & editing, Writing – original draft, Methodology, Investigation. **Erdal Özbek:** Writing – review & editing, Writing – original draft, Methodology. **Hakan Temiz:** Writing – review & editing, Writing – original draft, Methodology, Investigation. **Servet Tural:** Writing – review & editing, Writing – original draft, Visualization, Methodology, Investigation, Formal analysis, Conceptualization.

Ethical Approval

The study was conducted in accordance with the Declaration of Helsinki (2013 revision) and approved by the Dicle University Faculty of Medicine Non-Interventional Clinical Research Ethics Committee (Approval No: 14.11.2019–244).

Funding

No funding was received for this study.

Declaration of Competing Interest

The authors declare the following financial interests/personal relationships which may be considered as potential competing interests. Bilsen Tural has patent #Rapid and Easy Diagnosis of Tuberculosis Using Agents Attached to Magnetic Nanoparticles (original title in Turkish: "Manyetik Nanoparçacıklara Tutturulmuş Ajanlarla Tüberkülozun Hızlı ve Kolay Tanısı"), TR 2020 01710 B issued to Turkish Patent and Trademark Office. If there are other authors, they declare that they have no known competing financial interests or personal relationships that could have appeared to influence the work reported in this paper.

Acknowledgments

The authors extend their sincere gratitude to the Dicle University Scientific Research Coordination Unit (DUBAP) for supporting numerous projects, including project numbers ZGEF.24.012 and ZGEF.24.008.

Appendix A. Supporting information

Supplementary data associated with this article can be found in the online version at doi:10.1016/j.jpba.2025.117329.

Data Availability

The datasets generated and/or analyzed during the current study are available from the corresponding author upon reasonable request. Supplementary data containing supporting analytical results are provided with this article.

References

[1] W. Jaroenram, J. Kampeera, N. Arunrut, C. Karuwan, A. Sappat, P. Khumwan, W. Kiatpathomchai, Graphene-based electrochemical genosensor incorporated loop-mediated isothermal amplification for rapid on-site detection of *Mycobacterium tuberculosis*, J. Pharm. Biomed. Anal. 186 (2020) 113333, https://doi.org/10.1016/j.jpba.2020.113333.

[2] L. Wu, Z. Ye, H. Liu, H. Guo, J. Lin, L. Zheng, X. Liu, Rapid and highly sensitive quantification of the anti-tuberculosis agents isoniazid, ethambutol, pyrazinamide, rifampicin and rifabutin in human plasma by UPLC-MS/MS, J. Pharm. Biomed. Anal. 180 (2020) 113076, https://doi.org/10.1016/j.jpba.2019.113076.

[3] A.K. Gupta, A. Singh, S. Singh, Diagnosis of tuberculosis: nanodiagnostics approaches, Nano Bio. Med. (2020) 261–283, https://doi.org/10.1007/978-981-32-9898-9_11.

[4] E. MacLean, M. Kohli, S.F. Weber, A. Suresh, S.G. Schumacher, C.M. Denkinger, M. Pai, Advances in molecular diagnosis of tuberculosis, J. Clin. Microbiol. 58 (10) (2020) 10–1128, https://doi.org/10.1128/jcm.01582-19.

[5] N. León-Janampa, S. Shinkaruk, R.H. Gilman, D.E. Kirwan, E. Fouquet, M. Szlosek, M. Zimic, Biorecognition and detection of antigens from *Mycobacterium tuberculosis* using a sandwich ELISA associated with magnetic nanoparticles, J. Pharm. Biomed. Anal. 215 (2022) 114749, https://doi.org/10.1016/j.jpba.2022.114749.

[6] S.D. Lawn, M.P. Nicol, Xpert®MTB/RIF assay: development, evaluation and implementation of a new rapid molecular diagnostic for tuberculosis and rifampicin resistance, Future Microbiol 6 (9) (2011) 1067–1082, https://doi.org/10.2217/fmb.11.84.

[7] C.C. Boehme, P. Nabeta, D. Hillemann, M.P. Nicol, S. Shenai, F. Krapp, M. D. Perkins, Rapid molecular detection of tuberculosis and rifampin resistance, N. Engl. J. Med. 363 (11) (2010) 1005–1015, https://doi.org/10.1056/NEJMoa0907847.

[8] J. Nourry, P. Chevalier, E. Laurenceau, X. Cattoen, X. Bertrand, B. Peres, L. Choisnard, Whole-cell aptamer-based techniques for rapid bacterial detection: alternatives to traditional methods, J. Pharm. Biomed. Anal. (2025) 116661, https://doi.org/10.1016/j.jpba.2025.116661.

[9] J.K. Actor, Trehalose dimycolate (cord factor) as a contributing factor to tuberculosis pathogenesis. Tuberculosis Host-Pathogen Interactions, Springer International Publishing, Cham, 2019, pp. 43–61.

[10] B.U. Jaki, S.G. Franzblau, S.H. Cho, G.F. Pauli, Development of an extraction method for mycobacterial metabolome analysis, J. Pharm. Biomed. Anal. 41 (1) (2006) 196–200, https://doi.org/10.1016/j.jpba.2005.10.022.

[11] M. Walmagh, R. Zhao, T. Desmet, Trehalose analogues: latest insights in properties and biocatalytic production, Int. J. Mol. Sci. 16 (6) (2015) 13729–13745, https://doi.org/10.3390/ijms160613729.

[12] J. Zhu, H. Wang, L. Chen, Recent advances in nanomaterials for the detection of *Mycobacterium tuberculosis*, Int. J. Mol. Med 55 (3) (2024) 36, https://doi.org/10.3892/ijmm.2024.5477.

[13] E. Ahmadian, M. Samiei, A. Hasanzadeh, T. Kavetskyy, S. Jafari, M. Alipour, M. Hasanzadeh, Monitoring of drug resistance towards reducing the toxicity of pharmaceutical compounds: past, present and future, J. Pharm. Biomed. Anal. 186 (2020) 113265, https://doi.org/10.1016/j.jpba.2020.113265.

[14] S. Laurent, D. Forge, M. Port, A. Roch, C. Robic, L. Vander Elst, R.N. Muller, Magnetic iron oxide nanoparticles: synthesis, stabilization, vectorization, physicochemical characterizations, and biological applications, Chem. Rev. 108 (6) (2008) 2064–2110, https://doi.org/10.1021/cr068445e.

[15] I. Sant'Anna, R.,S. Arêdes, W.C.P. de Souza, R.C. da Silva Lessa, M.C. de Moraes, Development of an immobilized Mycobacterium tuberculosis purine nucleoside phosphorylase platform for ligand fishing and inhibition assays, J. Pharm. Biomed. Anal. 254 (2025) 116576, https://doi.org/10.1016/j.jpba.2024.116576.

[16] A.K. Gupta, M. Gupta, Synthesis and surface engineering of iron oxide nanoparticles for biomedical applications, Biomater 26 (18) (2005) 3995–4021, https://doi.org/10.1016/j.bio-materials.2004.10.012.

[17] S. Ahmadi, F.R. Sedaghat, M.Y. Memar, M. Yekani, Metabolomics in the diagnosis of bacterial infections, Clin. Chim. Acta (2024) 120020, https://doi.org/10.1016/j.cca.2024.120020.

[18] B.M. Swarts, C.M. Holsclaw, J.C. Jewett, M. Alber, D.M. Fox, M.S. Siegrist, C. R. Bertozzi, Probing the mycobacterial trehalome with bioorthogonal chemistry, J. Am. Chem. Soc. 134 (39) (2012) 16123–16126, https://doi.org/10.1021/ja3062419.

[19] S. Thanna, S.J. Sucheck, Targeting the trehalose utilization pathways of *Mycobacterium tuberculosis*, Med. Chem. Commun. 7 (1) (2016) 69–85, https://doi.org/10.1039/C5MD00–376 H.

[20] K.W. Jayawardana, N. Kong, Y. Ren, N. Hao, M. Yan, O. Ramström, Trehalose-conjugated, photofunctionalized mesoporous silica nanoparticles for efficient delivery of isoniazid into mycobacteria, ACS Biomater. Sci. Eng. 1 (12) (2015) 1250–1255, https://doi.org/10.1021/acsbiomaterials.5b00274.

[21] P.C. Martian, M. Tertis, D. Leonte, N. Hadade, C. Cristea, O. Crisan, Cyclic peptides: a powerful instrument for advancing biomedical nanotechnologies and drug development, J. Pharm. Biomed. Anal. 252 (2025) 116488, https://doi.org/10.1016/j.jpba.2024.116488.

[22] Rapid and simple diagnosis of tuberculosis using agents immobilized on magnetic nanoparticles, Turkish Patent TR 2020/01710, Turkish Patent and Trademark Office, issued 2024.

[23] K. Kolbe, L. Möckl, V. Sohst, J. Brandenburg, R. Engel, S. Malm, N. Reiling, Azido pentoses: a new tool to efficiently label *Mycobacterium tuberculosis* clinical isolates, Chem. Bio. Chem. 18 (13) (2017) 1172–1176, https://doi.org/10.1002/cbic.201600-706.

[24] M. Lin, Y.W. Chen, Y.R. Li, L.J. Long, L.Y. Qi, T.T. Cui, X.G. Guo, Systematic evaluation of line probe assays for the diagnosis of tuberculosis and drug-resistant tuberculosis, Clin. Chim. Acta 533 (2022) 183–218, https://doi.org/10.1016/j.cca.2022.06.020.

[25] S. Tural, M. Ece, B. Tural, Synthesis of novel magnetic nano-sorbent functionalized with N-methyl-D-glucamine by click chemistry and removal of boron with magnetic separation method, Ecotoxicol. Environ. Saf. 162 (2018) 245–252, https://doi.org/10.1016/j.ecoenv.2018.06.066.

[26] E. Bianchetti, C. Di Valentin, Effect of surface functionalization on the magnetization of Fe_3O_4 nanoparticles by hybrid density functional theory calculations, J. Phys. Chem. Lett. 13 (40) (2022) 9348–9354, https://doi.org/10.1021/acs.jpclett.2c02186.

[27] S. Dagher, A. Soliman, A. Ziout, N. Tit, A. Hilal-Alnaqbi, S. Khashan, J.A. Qudeiri, Photocatalytic removal of methylene blue using titania-and silica-coated magnetic nanoparticles, Mater. Res. Express 5 (6) (2018) 065518, https://doi.org/10.1088/2053-1591/aacad4.

[28] X. Ji, R. Qiao, Z. Xu, J. Liu, Q. Ma, H. Yuan, H. Xing, Synthesis of Fe_3O_4/SiO_2 nanocomposites via click chemistry and electromagnetic wave absorption properties, J. Mater. Sci. Mater. Electron 35 (15) (2024) 1004, https://doi.org/10.1007/s10854-024-12766-3.

[29] R.M. Fratila, M. Navascuez, J. Idiago-López, M. Eceiza, J.I. Miranda, J. M. Aizpurua, J.M. de la Fuente, Covalent immobilisation of magnetic nanoparticles on surfaces via strain-promoted azide–alkyne click chemistry, N. J. Chem. 41 (19) (2017) 10835–10840, https://doi.org/10.1039/C7NJ01822C.

[30] M. Paciorek, A. Pihowicz, D. Bursa, J.S. Humięcka, J.D. Kowalska, M. Antosiewicz, A. Horban, Prior treatment with non anti-TB antibiotics, and the duration of symptoms have no effect on diagnostics of *Tuberculous meningitis*, Adv. Med. Sci. 62 (2) (2017) 374–377, https://doi.org/10.1016/j.advms.2016.11.003.

[31] N. Singh, B. Dahiya, V.S. Radhakrishnan, T. Prasad, P.K. Mehta, Detection of *Mycobacterium tuberculosis* purified ESAT-6 (Rv3875) by magnetic bead-coupled gold nanoparticle-based immuno-PCR assay, Int. J. Nanomed. 13 (2018) 8523–8535, https://doi.org/10.2147/IJN.S181052.

[32] N. León-Janampa, M. Zimic, S. Shinkaruk, J. Quispe-Marcatoma, A. Gutarra, G. Le Bourdon, M. Szlosek, Synthesis, characterization and bio-functionalization of magnetic nanoparticles to improve the diagnosis of tuberculosis, Nanotechnol 31 (17) (2020) 175101, https://doi.org/10.1088/1361-6528/ab6ab1.

[33] N. Bhusal, S. Shrestha, N. Pote, E.C. Alocilja, Nanoparticle-based biosensing of tuberculosis, an affordable and practical alternative to current methods, Biosens 9 (1) (2018) 1, https://doi.org/10.3390/bios9010001.

[34] H.J. Kim, J. Rim, C.H. Jang, Liquid-crystal-based immunosensor for diagnosis of tuberculosis in clinical specimens, ACS Appl. Mater. Interfaces 9 (25) (2017) 21209–21215, https://doi.org/10.1021/acsami.7b06189.

[35] J. Zhou, K.W. Jayawardana, N. Kong, Y. Ren, N. Hao, M. Yan, O. Ramström, Trehalose-conjugated, photofunctionalized mesoporous silica nanoparticles for efficient delivery of isoniazid into mycobacteria, ACS Biomater. Sci. Eng. 1 (12) (2015) 1250–1255, https://doi.org/10.1021/acsbio-materials.5b00274.

[36] L.H. Liu, H. Dietsch, P. Schurtenberger, M. Yan, Photoinitiated coupling of unmodified monosaccharides to iron oxide nanoparticles for sensing proteins and bacteria, Bioconjugate Chem. 20 (7) (2009) 1349–1355, https://doi.org/10.1021/bc900110x.

[37] X. Zhang, X. He, L. Chen, Y. Zhang, Boronic acid modified magnetic nanoparticles for enrichment of glycoproteins via azide and alkyne click chemistry, J. Mater. Chem. 22 (32) (2012) 16520–16526, https://doi.org/10.1039/C2JM32987E.

[38] P.J. Brennan, Structure, function, and biogenesis of the cell wall of *Mycobacterium tuberculosis*, Tuberculosis 83 (1-3) (2003) 91–97, https://doi.org/10.1016/S1472-9792(02)00089-6.

[39] K. Takayama, C. Wang, G.S. Besra, Pathway to synthesis and processing of mycolic acids in *Mycobacterium tuberculosis*, Clin. Microbiol. Rev. 18 (1) (2005) 81–101, https://doi.org/10.1128/cmr.18.1.81-101.2005.

[40] Y. Yuan, R.E. Lee, G.S. Besra, J.T. Belisle, C.E. Barry 3rd, Identification of a gene involved in the biosynthesis of cyclopropanated mycolic acids in *Mycobacterium tuberculosis*, Proc. Natl. Acad. Sci. 92 (14) (1995) 6630–6634.

[41] S. Gautam, T.J. Gniadek, T. Kim, D.A. Spiegel, Exterior design: strategies for redecorating the bacterial surface with small molecules, Trends Biotechnol. 31 (4) (2013) 258–267, https://doi.org/10.1016/j.tibtech.2013.01.012.

[42] A. Duque, S.Y.G. Lin, E. Desmond, S. Rienthong, D. Rienthong, C. Boonin, Evaluation of the BD Bactec MGIT 320 system for detection of mycobacteria and drug susceptibility testing of Mycobacterium tuberculosis, J. Clin. Microbiol. 51 (10) (2013) 3403–3405, https://doi.org/10.1128/jcm.01357-13.

[43] D. Tayal, P. Sethi, P. Jain, Point-of-care test for tuberculosis: a boon in diagnosis, Monaldi. Arch. Chest. Dis. 94 (1) (2024), https://doi.org/10.4081/monaldi.2023.2528.